Energy-resolved momentum densities for the valence band of a nanoscale Si single crystal

2000 J. Phys.: Condens. Matter 12 125

(http://iopscience.iop.org/0953-8984/12/2/303)

J. Phys.: Condens. Matter **12** (2000) 125–136. Printed in the UK PII: S0953-8984(00)08026-7

Energy-resolved momentum densities for the valence band of a nanoscale Si single crystal

V A Sashin†, S A Canney†§, M J Ford†, M A Bolorizadeh†, D R Oliver† and A S Kheifets‡

† Physics Department, Flinders University, GPO Box 2100, SA 5001, Australia
‡ Research School of Physical Sciences and Engineering, Institute of Advanced Studies, ANU, Canberra, ACT 0200, Australia

E-mail: michael.ford@flinders.edu.au

Received 21 September 1999

Abstract. We have measured the energy- and momentum-resolved band structure, and ground state of occupation of the bands, for a crystalline silicon sample along the ⟨100⟩ and ⟨110⟩ directions. Band structures were determined directly by the technique of electron momentum spectroscopy (EMS) for a self-supporting Si membrane with a thickness of approximately 7 nm. We compare our experimental results with *ab initio* calculations for bulk crystalline silicon performed within the linear muffin tin orbital approximation. Qualitative agreement is seen between experiment and theory for the main valence band peak. Additional intensity is observed in the measurement on either side of the main peak and is attributed mainly to multiple-scattering events. Satellite structure could also be present in these additional features, although there is no direct evidence for this.

1. Introduction

The band dispersion relations together with the occupation of states within the bands provides a complete picture of the electronic structure, and has a direct bearing upon the physical and chemical properties, of the condensed phase of matter. In addition, experimentally determined electron-momentum densities can provide a very sensitive test of the validity of currently available theoretical schemes used to calculate electronic structures. For these reasons, and because of its technological importance, a large body of literature has evolved reporting experimental and theoretical studies of the electronic structure of Si and Si-based systems.

Photon impact techniques are widely used to probe the electronic structure of solids. Photoelectron spectroscopy determines the energy-resolved density of states. Energy–momentum dispersion relations for occupied bands can often be inferred reliably from angle-resolved measurements [1], provided certain assumptions regarding the final state of the photoelectron are valid, essentially that the sample is a single crystal with a flat surface. In a similar manner, inverse photoemission can yield band dispersions for unoccupied states [2]. Compton scattering experiments provide information on the momentum densities projected onto a particular crystal direction but integrated over energy, and can be used to investigate the fermiology of metals [3]. The dispersion relations for Si over a range of bands have been mapped using photoemission techniques [4–8]. A number of theoretical treatments of the Si band structure are reported in the literature, ranging from plane-wave models to tight binding

§ Present address: Defence Science and Technology Organization, PO Box 1500, Salisbury, SA 5108, Australia.

0953-8984/00/020125+12$30.00

calculations and diffusion quantum Monte Carlo techniques [9–13]. Comparison between theory and experiment, however, has largely been limited to comparing the energies of only a few special points within the band structure.

More recently electron impact techniques, developed for mapping wavefunctions of atomic and molecular targets [14], have been applied to the solid state. Electron-momentum spectroscopy (EMS) measures the real momentum of the target electrons rather than crystal momentum (as is the case in photoemission experiments) and can determine directly, and simultaneously, both the band dispersions and occupied states within the bands, i.e. the full energy-resolved momentum density [15]. The technique has great potential for determining electronic properties at a fundamental level for an extremely wide range of materials, both amorphous, polycrystalline and crystalline. To date, energy–momentum densities have been measured by EMS almost exclusively for amorphous and polycrystalline targets [16]. Measurements have been reported for crystalline graphite [17], and an investigation of diffraction effects in EMS from a crystalline Si target has been performed by Fang *et al* [18]. The electronic structure of Si measured by EMS has, so far, only been reported for the amorphous state [19]. Comparison with theory in this experiment required spherical averaging of the calculated crystal band structure to account for the disordered nature of the target, a procedure that results in partial loss of information from the theory and introduces some ambiguity into the comparison.

In this paper we present EMS measurements of the energy-resolved momentum densities of a single-crystal Si target along the high symmetry crystal directions $\langle 100 \rangle$ and $\langle 110 \rangle$. Our experimental results provide the first opportunity to make a complete and direct comparison with the calculated electronic structure of Si. We compare our experimental results with calculations performed within the linear muffin tin orbital (LMTO) approximation.

2. Experiment

Electron-momentum spectroscopy uses electron impact ionization to map the target electron energy–momentum density. Under the appropriate kinematics (where the momentum transferred from the incident to target electron is large) the ionization process is essentially a billiard-ball-like collision—the so-called (e, 2e) event [15]. In the experiment the incident electron energy and momentum is well defined, and the energies and momenta of the outgoing scattered-incident and ejected-target electrons are measured. Conservation of energy and momentum then determines the binding energy ε and momentum $\boldsymbol{q}$ of the target electron immediately before the ionization event. The density of target electrons (square of the momentum–energy space wavefunction) is mapped by detecting the two outgoing electrons over a range of azimuthal angles and energies simultaneously. The detection range of our spectrometer has been designed so that the energy–momentum density can be mapped along a single crystal direction (the y-axis in figure 1). The time correlation of the two outgoing electrons is also measured (coincidence detection); electrons originating from the same (e, 2e) event will essentially be detected at the same time. By this method we can extract the small signal due to true (e, 2e) events from a large background of other scattering processes.

Our spectrometer [20] uses an asymmetric geometry with incident, fast-scattered and slow-ejected energies of nominally 20.8 keV, 19.6 keV and 1.2 keV respectively. The polar angles at which the outgoing electrons are detected are fixed at 13.6 (fast scattered) and 76° (slow ejected). The scattering geometry is shown schematically in figures 1(a) and (b). Two-dimensional position sensitive detectors mounted on the exit apertures of the electron energy analysers allow us to collect data over a range of azimuthal angles and energies in a single experiment. The incoming or outgoing electrons of an (e, 2e) event which undergo additional

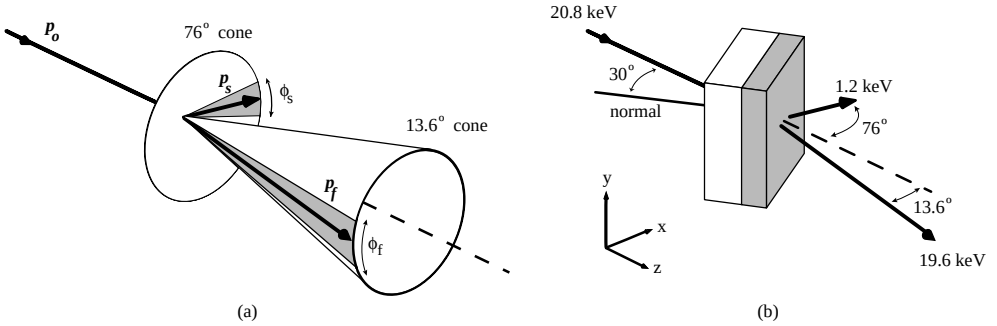

Figure 1. Scattering geometry of the spectrometer. In (a) the range of detected electron angles is shown and in (b) sample orientation with respect to the incident and outgoing electrons is shown. The shaded area in (b) indicates the region of the sample that contributes most to the measured energy–momentum density.

small angle elastic, or inelastic, collisions can also give rise to coincidence events. These processes generate events which are shifted along the momentum axis for elastic collisions and both the momentum and energy axes for inelastic collisions. They produce a smooth, random background to the measurement together with ghost images of the band-structure due to plasmon excitation. The experiment is performed in transmission mode and requires extremely thin targets (of the order of 10 nm) to avoid the (e, 2e) signal being dominated by this multiple-scattering background.

With a single-crystal sample, diffraction of the incoming or outgoing electrons can potentially complicate measurements of the electronic structure of the target. A detailed experimental and theoretical investigation of diffraction in EMS has been performed by Fang *et al* [18]. Rotation of the sample around the y-axis in figure 1 changes the contribution of diffraction to the EMS signal. The measured signal-to-background ratio is also strongly dependent upon orientation about this axis, even to the extent that the signal is practically lost in the background for certain orientations. Introducing a small tilt angle of the sample around the x-axis can reduce diffraction to a negligible level. This is not desirable for the present measurements however, because it would shift the direction in which the momentum is sampled out of the plane of the target, giving rise to contributions from crystal directions other than those intended. In the spectrometer the Si target is attached to a manipulator which provides accurate xyz translation and rotation about the y- and z-axes only. By rotating around the z-axis different crystal directions can be measured; the actual orientation of the crystal with respect to the y-axis is determined from the *in situ* electron transmission diffraction pattern. Rotation around the x-axis is constrained mechanically and can be fixed at a given angle to an accuracy of a few degrees. To minimize diffraction effects in the EMS measurement and maximize the signal-to-background ratio we rotate around the y-axis by 30°. As noted above the rotation around the x-axis is fixed as accurately as possible to zero. Under these conditions, Fang *et al* [18] calculate that the undiffracted signal contributes 74% of the total signal.

The targets used in the spectrometer need to be ultra-thin and self-supporting over a diameter at least as large as the incident electron beam (0.2 mm). We prepare our Si samples from standard wafers using a combination of wet-chemical, and plasma etching with CF_4/O_2 gas mixtures. The samples are thinned on only one side—the side which faces the incident electron beam (see figure 1(b)). Once the membrane has been thinned to its final thickness, it is annealed gently to remove fluorine contamination of the surface that results from the plasma etching stage. Membrane thickness during the plasma etch is monitored from the

transmitted intensity of an He–Ne laser beam. The estimated thickness of the membranes used in the present work is approximately 7 nm. Sample preparation and characterization are described in detail in a separate paper [21]. Plasma etching and annealing are carried out in separate chambers attached to the main measurement chamber. All chambers are equipped with transfer arms allowing the sample to be moved between the plasma etching, annealing and measurement chambers under UHV conditions. The annealing temperature is of the order of several hundred degrees. The extreme thinness of the sample and the use of a bare filament for annealing excludes the use of an optical pyrometer to estimate annealing temperatures more accurately. In most cases the samples show very good bulk crystallinity (determined by electron transmission diffraction) even before the annealing process. For a few cases where faint rings were present in the diffraction pattern, gentle annealing as described above was sufficient to remove the presence of these rings. The Auger electron spectrum of a typical sample, immediately after annealing, is shown in figure 2(a). This measurement is performed *in situ* using an electron energy analyser separate from the main EMS spectrometer. Only a small amount of carbon and oxygen contamination is evident in the spectrum. The EMS measurement is performed under UHV conditions (approximately 10^{-10} Torr), and takes approximately 3 days to acquire sufficient statistics. Even under these conditions, the sample surface shows a slight increase in surface contamination: the Auger spectrum immediately after a measurement is shown in figure 2(b). The escape depth of the slow-ejected electron means that the measurement is sensitive to the outermost 2 nm of the target (figure 1(b)): the measurement is therefore not as sensitive to small amounts of surface contamination.

3. Theory

Calculations of the band dispersions and electron-momentum densities (EMDs) have been performed using the liner muffin tin orbital (LMTO) method within the atomic sphere approximation. The formalism of this method is described by Skriver [22]. The basis of this method is to substitute the atomic polyhedra with an atomic sphere for each non-equivalent atomic position. The muffin tin (MT) radius of a sphere at site s, R_s, is then estimated by setting the total volume of the spheres equal to the volume of the unit cell, Ω

$$\sum_s \frac{4}{3}\pi R_s^3 = \Omega. \tag{1}$$

Inside the spheres the electron potential is spherically symmetric, and the tails of the LMTO orbitals outside the spheres are assigned to have zero kinetic energy. Within the spheres the Bloch sum of the tails is cancelled, and the one-electron wavefunction for a given sphere centred at $\boldsymbol{r}_s$ is written as

$$\psi_{jk}(\boldsymbol{r}-\boldsymbol{r}_s) = \sum a_{slm}^{jk} i^l Y_{lm}(\hat{r}_1)\frac{1}{r_1}P_{sl}(r_1) \qquad r_1 = |\boldsymbol{r}-\boldsymbol{r}_s| \leqslant R_s \tag{2}$$

where $\boldsymbol{k}$ is the crystal wavevector, j is the band index and Y_{lm} is the spherical harmonic which depends on the orbital momentum l and its projection m. The expansion coefficients a_{slm}^{jk} are found by solving the LMTO eigenvalue equation. The radial part of the wavefunction $P_{sl}(r)$ depends on the atom type at site s and the orbital momentum l. The computational efficiency of this method is greatly increased by the fact that the wavefunction $P_{sl}(r)$ is independent of $\boldsymbol{k}$ and j.

The Si unit cell has two non-equivalent atomic positions at $(0, 0, 0)$ and $(a/4, a/4, a/4)$ where a is the lattice parameter. To treat this very open structure (the packing fraction is only 0.34) we follow Glötzel *et al* [23] and place two empty atomic spheres at the interstitial sites $(-a/4, -a/4, -a/4)$ and $(a/2, 0, 0)$.

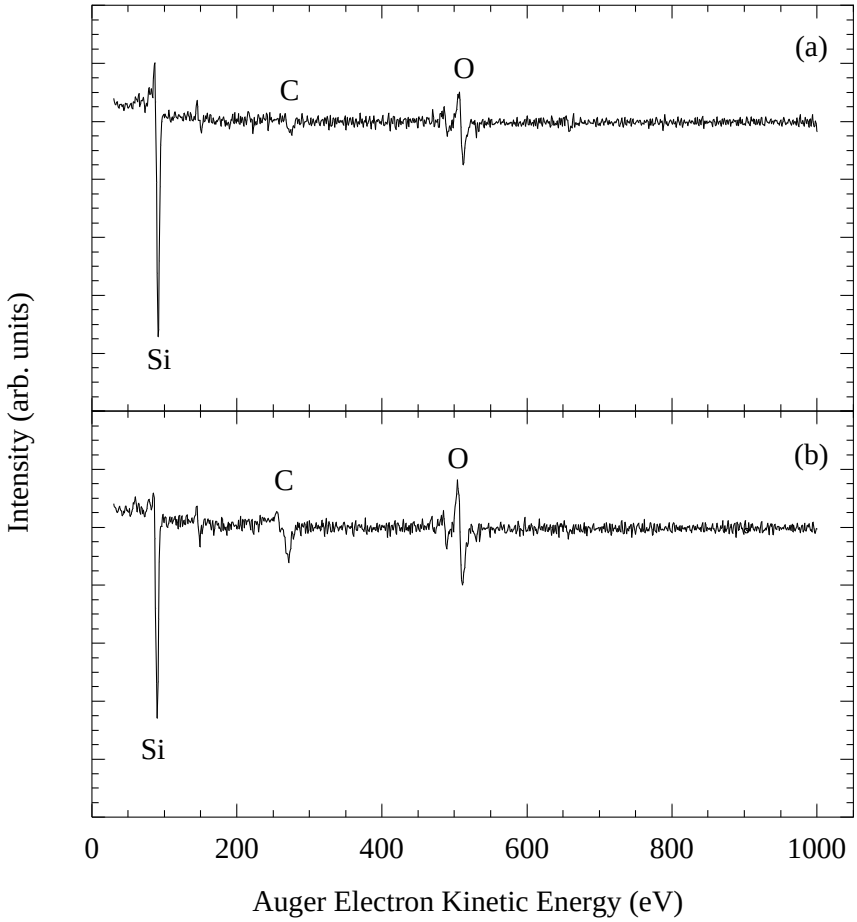

Figure 2. Differential Auger electron energy spectra for the Si target, (a) immediately after annealing and before the EMS measurement and (b) immediately after the measurement.

The MT radius is then calculated for four equal size spheres from (1) as

$$R_s = \frac{a}{4}\left(\frac{3}{\pi}\right)^{1/3} = 0.2462a = 1.337 \text{ Å} \tag{3}$$

where $a = 5.431$ Å [24].

Details of the calculation and plots of the band dispersions and EMDs are given in the paper by Kheifets and Cai [12].

4. Results

Grey-scale plots of the measured and calculated energy–momentum densities for the Si valence band along the ⟨100⟩ and ⟨110⟩ directions are presented in figures 3(a) and (b) respectively. Conventionally, band-dispersions are plotted in terms of the special points of the Brillouin zone in the reduced zone scheme. Because we measure the real momentum of the target electrons in the present experiment, our band structures are plotted with respect to electron momentum and are in the extended zone scheme. The calculation has been convoluted with Gaussians

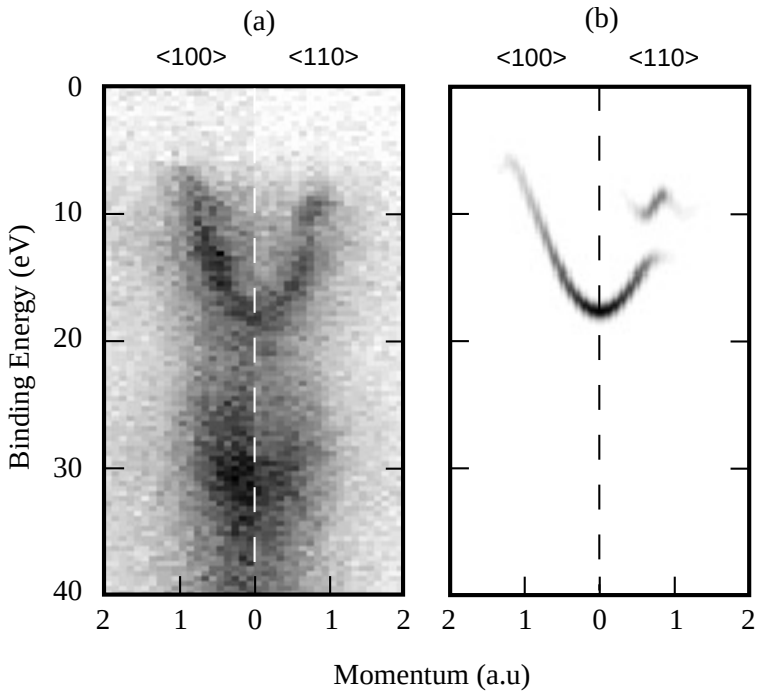

Figure 3. Energy-resolved momentum densities for Si along the ⟨100⟩ and ⟨110⟩ directions determined by (a) experiment and (b) the LMTO method. Intensity is on a linear grey scale with darker colour representing higher intensity.

of 1.0 eV (FWHM) and 0.1 au (FWHM) to match the experimental energy and momentum resolutions respectively. Zero binding energy in the experimental results corresponds to the vacuum level, whereas the calculation is referenced to the valence band maximum. The calculation has, therefore, been shifted by approximately 5 eV to align the Γ point of the lower valence band with the experiment. The experimental results contain a substantial background due to elastic and inelastic multiple scattering experienced by the electrons comprising the (e, 2e) signal. These events have not been taken account of in the calculation. Inelastic scattering provides an additional energy-loss mechanism for the (e, 2e) electrons and produces the observed intensity below the bottom of the valence band which peaks at approximately 30 eV. Qualitative agreement can be seen between the experimental and theoretical valence band structures for both crystal directions. Along the ⟨100⟩ direction the band dispersion follows a free-electron-like parabola, whereas in the ⟨110⟩ an intervalence bandgap opens up at a momentum of around 0.6 au There is no noticeable contribution from diffracted signals: this would produce a reflection of the valence band shifted along the momentum axis [18]. For the target orientation used in the present experiments one might expect to observe slight diffraction effects. Their absence is not due to disorder in the sample: the electron transmission diffraction pattern is indicative of a highly crystalline structure [21]. They are most likely lost in the background of the measurement, or are not present because of the slight inaccuracy of the rotation set around the x-axis.

A more quantitative comparison can be made by taking vertical slices through the energy–momentum densities of figure 3 summed over an appropriate momentum range. The experiment samples both positive and negative momentum values along the y-axis. Since the energy–momentum density is symmetric about zero momentum, the negative and positive

momentum components have been added together to improve the statistics. The resulting binding energy curves, integrated over 0.2 au momentum intervals, are shown in figures 4 and 5 for the ⟨100⟩ and ⟨110⟩ directions respectively. The experimental and calculated valence band peaks have been normalized in the momentum interval $0.0 < \boldsymbol{q} < 0.2$ au for the ⟨100⟩ direction and $0.2 < \boldsymbol{q} < 0.4$ for the ⟨110⟩ direction.

For the ⟨100⟩ direction the experimental data (figure 4) show a binding energy peak at approximately 18 eV at zero momentum which disperses to lower energy as the momentum increases. This overall behaviour is reproduced in the calculated spectra. However, there is also considerable intensity either side of this peak in the experimental data that is not present in the calculation (the calculation includes no contribution from multiple scattering). Intensity on the low energy side of the main peak most likely arises from multiple scattering where the (e, 2e) electrons undergo a small angle elastic scattering event. This results in a change in momentum of one of the electrons which shifts intensity along the momentum axis. In this manner some additional intensity is produced on either side of the valence band feature in the energy–momentum density. The same result was observed by Vos *et al* [19] for their EMS measurements on amorphous silicon, and the authors suggest this structure cannot be due to the disordered nature of the target. The authors further suggest that satellite states could be responsible for the intensity at low binding energies. This seems unlikely given that satellite structures usually occur on the high binding energy side of the main valence peak, and that similar features have been observed in EMS measurements on a range of targets. However, for metallic targets such as Mg [25] and Al [26], this effect is much less pronounced than is the case for the present measurements. In addition a small peak is observed for intermediate momentum values at approximately 10 eV: the possible origin of this peak is discussed below.

A broader peak is also observed in figure 4 on the high binding energy side of the valence band at approximately 30 eV. Once again this can be attributed to multiple scattering, this time from one of the (e, 2e) electrons undergoing an inelastic process such as excitation of a plasmon or a valence band electron. If the main contribution to this feature arises from excitation of a single plasmon, the peak should occur at an energy loss below the valence band equal to the plasmon excitation energy. The peak position should also disperse along with the valence band peak as the momentum increases; this behaviour is not observed in our results. We have measured the electron energy-loss spectrum for the Si target for an incident energy of 19.6 keV and scattering angle of 13.6°: the result is shown in figure 6. Two energy-loss peaks are present at approximately 17 eV and 34 eV corresponding to excitation of one and two plasmons respectively. This would imply that the high binding energy feature in figure 4 should appear at 35 eV (for zero momentum) if it is indeed due to excitation of a single plasmon. The high binding energy feature cannot be described simply by excitation of a single plasmon. Other processes, such as excitation of valence electrons, or satellite states make a significant contribution. By comparison, our results for Mg [25] show features that can clearly be identified as arising from plasmon excitation.

Binding energy spectra for the ⟨110⟩ direction (figure 5) clearly show the valence band gap that opens up at the Brilloun zone boundary around 0.6 au of momentum. The calculated dispersions of the main peaks are in good agreement with the experimental result. The background for this direction shows almost identical behaviour to the ⟨100⟩ direction, with considerable intensity below the main peak and a second, broader, peak centred at approximately 30 eV binding energy. This similarity is due to the fact that the thickness, which mainly determines the shape and intensity of the multiple-scattering background, is approximately the same for the two samples used. According to our estimates the thickness is 7.5 and 6.2 nm for the ⟨100⟩ and ⟨110⟩ measurements respectively (estimated from the transmitted intensity of the He–Ne laser).

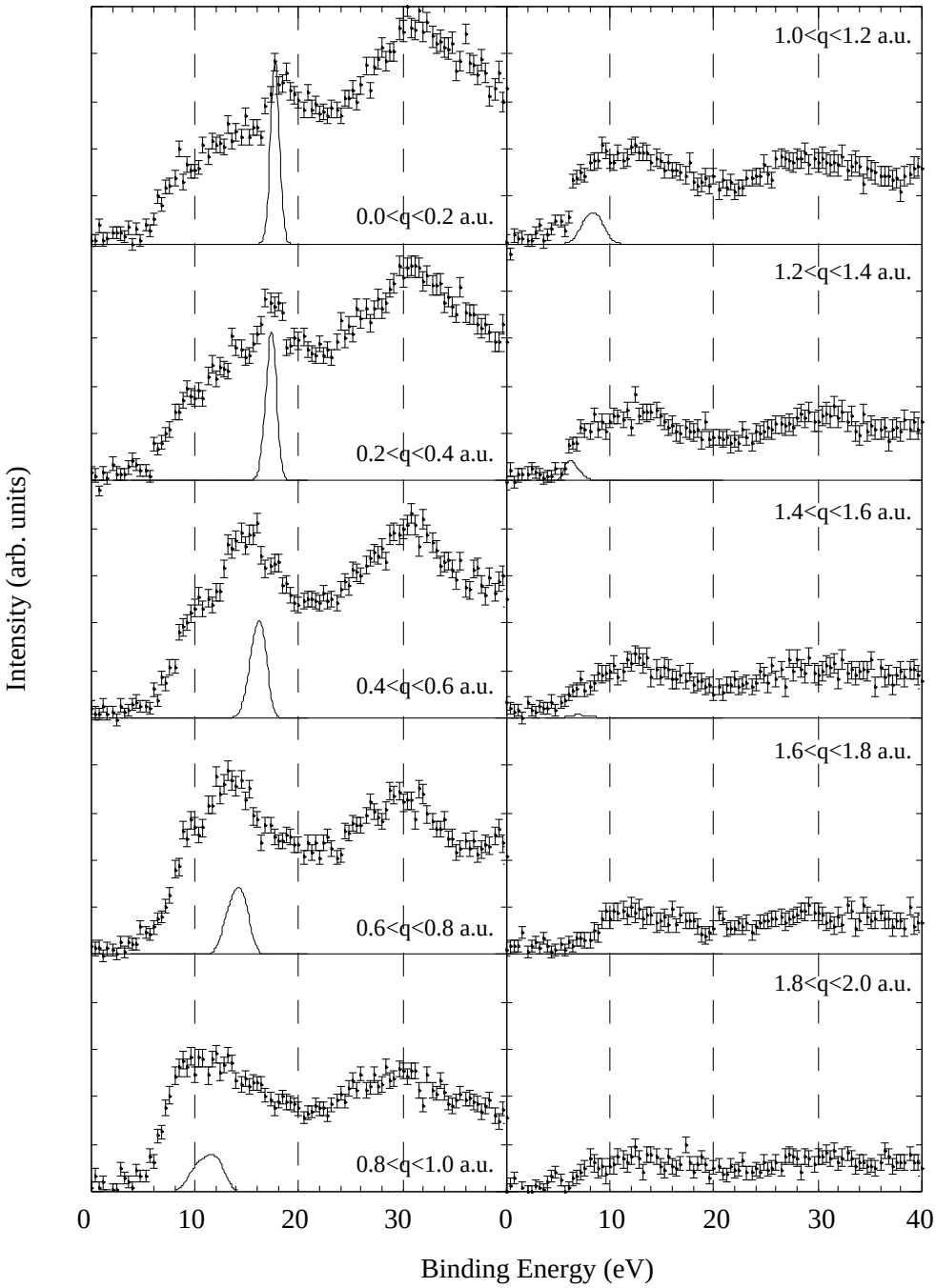

Figure 4. Binding energy spectra as a function of electron momentum in the ⟨100⟩ direction obtained by integrating the energy–momentum density over 0.2 au momentum intervals. Points with error bars are the experimental data; solid lines are the calculation.

Within the momentum interval $0.6 < q < 0.8$ au the second weak feature at approximately 10 eV observed in the ⟨100⟩ direction is comparable to the upper valence band peak in the

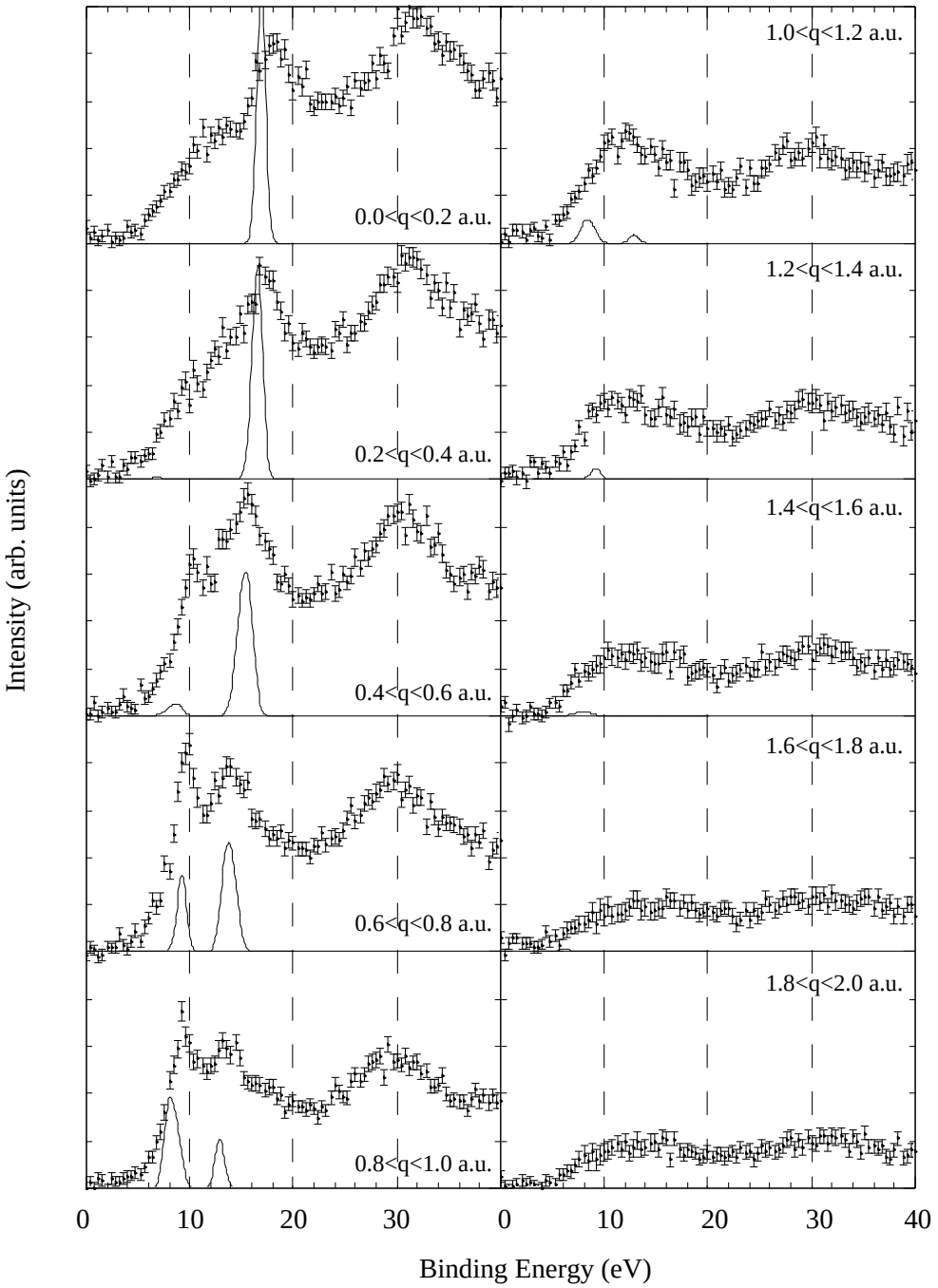

Figure 5. Binding energy spectra as a function of electron momentum in the ⟨110⟩ direction obtained by integrating the energy–momentum density over 0.2 au momentum intervals. Points with error bars are the experimental data; solid lines are the calculation.

⟨110⟩ direction. This raises the possibility that other directions are contributing to the ⟨100⟩ measurement. If this feature were due to disorder in the near-surface region of the sample

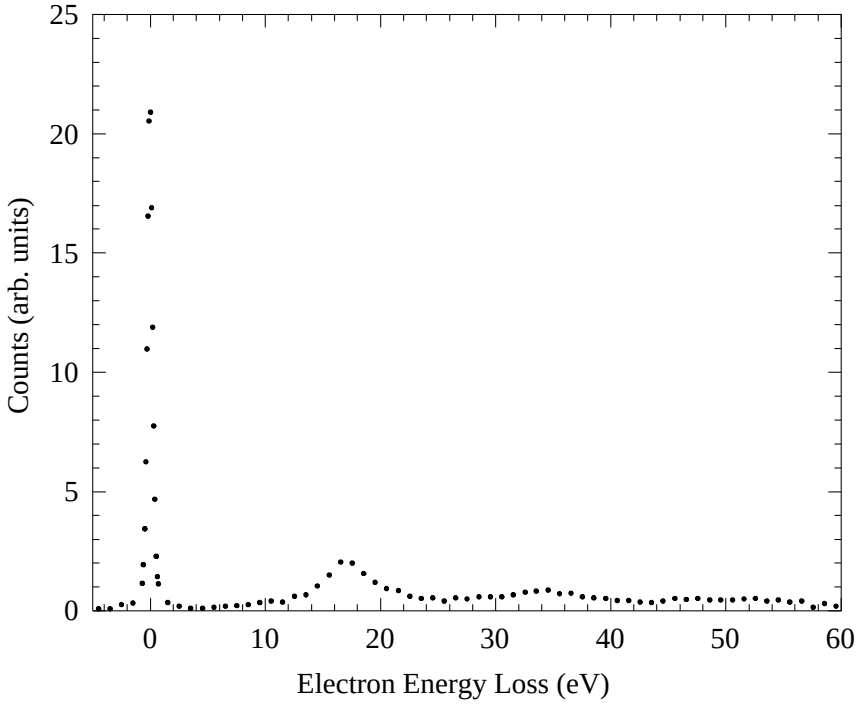

Figure 6. Electron energy-loss measurement for the Si membrane. Incident electron energy is 19.6 keV and the scattering angle is 13.6°.

one would not expect to see a second peak but rather a broadening of the main peak due to equal contributions from many crystal directions, as is observed for amorphous Si [19]. We orient a particular crystal axis relative to the measurement direction (the y-axis) by observing the diffraction pattern and rotating around the z-axis. This can be done accurately. However, there can still be a small mechanical misalignment with respect to rotation around the x-axis. In addition, from the scattering geometry we know that the measurement is not strictly along the y-axis of the experiment (see figure 1) but can also contain a small contribution along the x-axis. This contribution reaches a maximum of approximately 0.1 au at intermediate momentum values. The uncertainty that this introduces into the measurement direction is relatively small, but may be sufficient, together with misalignment around the x-axis, to introduce small contributions from directions away from $\langle 100 \rangle$. Energy–momentum densities from other directions may also make a small contribution to the $\langle 100 \rangle$ measurement due to diffraction effects.

From our measured and calculated binding energy spectra we can derive the energies of the Γ_1, X_1 and X_4 special points of the band dispersion. The Γ–X–Γ line in momentum space corresponds to the $\langle 100 \rangle$ direction, with the X point occurring at a momentum value of 0.61 au. The Γ–K–X–K–Γ line corresponds to the $\langle 110 \rangle$ direction, with the K point at 0.65 au and the X point at 0.87 au. Special point energies are presented in table 1 along with values obtained in previous experimental and theoretical works. Our experimental values are derived from binding energy spectra integrated over 0.1 au momentum intervals. The position of the valence band peak is found from a least squares fit using Gaussian functions. Energies in table 1 are relative to the valence band maximum; the experimental energies of the Γ_1 point have been shifted by 6.0 and 6.1 eV for the $\langle 100 \rangle$ and $\langle 110 \rangle$ directions respectively so they coincide with

the calculated value. Values for the X_1 point then agree to within 0.1 eV for the ⟨100⟩ and ⟨110⟩ directions. We estimate the error in our experimental values to be approximately 0.5 eV. The energies of the special points derived from our measurement are relatively consistent with our calculated values. Previously reported values are consistent amongst themselves and with our values except for the diffusion quantum Monte Carlo calculation of Williamson *et al* [13], where the values are consistently lower in energy, and the energy of the X_4 point measured by Wachs *et al* [4] to be −3.4 eV.

Table 1. Energies of selected special points (in eV) relative to the valence band maximum.

Γ_1	X_1	X_4	Method	Reference
−11.93	−7.75	−2.72	LMTO	Present
−11.93	−7.1	−3.1	Expt	Present
−11.87	−7.75	−2.72	LMTO	[23]
−12.36	−7.69	−2.86	EPM	[27]
−12.04	−8.01	−2.98	GWA	[11]
−13.58	−8.79	−3.35	DMC	[13]
−12.5			Expt	[28]
		−2.9	Expt	[29]
		−3.4	Expt	[4]

Our LMTO calculations have been performed for bulk Si whereas the sample used in measurement is less than 10 nm thick. Size effects are not expected to contribute to the measurement because the scattering geometry means that momentum is sampled essentially in the plane of the target. The data show no obvious indication of these effects.

5. Conclusion

We have measured the dispersion relation and intensities of the valence band of Si in the ⟨100⟩ and ⟨110⟩ directions using electron momentum spectroscopy. Dispersion of the main valence band peaks is in good agreement with our LMTO calculation of the band structure. Energies of the Γ_1, X_1 and X_4 special points derived from the measurement are also in good agreement with the present calculation and previous work.

Additional intensity is also observed on either side of the valence band peak and is attributed mainly to multiple scattering of the electrons. Small angle elastic scattering of one of the electrons involved in the (e, 2e) event results in intensity on the low binding energy side of the main peak. The intensity observed in this region is very large compared to our previous measurements of metallic solids such as Mg and Al. Inelastic scattering, such as plasmon excitation and single-electron excitation, produces intensity on the high binding energy side. In this region we observe a broad peak; however, the energy of this peak is not consistent with the energy loss required to excite a single (or multiple) plasmon. This is not consistent with previous measurements where energy loss features due to plasmon excitation are easily identified in the EMS measurement. Satellite states could produce intensity away from the main peak, especially on the high energy side, although we have no direct evidence that this is the case.

Multiple-scattering events need to be convoluted with the calculation, or equally deconvoluted out of the experiments. Achievement of either of these goals would lead to a greater understanding of the origin of the background intensity. We are in the process of developing a Monte Carlo procedure to do this. In addition, it would be informative to compare our measurements with calculations that include many-body effects.

Acknowledgments

This work was supported by grants from the Australian Research Council and Flinders University.

References

[1] Hansson G V and Uhrberg I G 1988 *Surf. Sci. Rep.* **9** 197
[2] Himpsel F J 1990 *Surf. Sci. Rep.* **12** 1
[3] Hämäläinen K, Manninen S, Kao C-C, Caliebe W, Hastings J B, Bansil A, Kaprzyk S and Platzman P M 1996 *Phys. Rev.* B **54** 5453
[4] Wachs A L, Miller T, Hsieh T C, Shapiro A P and Chiang T-C 1985 *Phys. Rev.* B **32** 2326
[5] Uhrberg R I G, Hansson G V, Karlsson U O, Nicholls J M, Persson E S, Flodström S A, Engelhardt R and Koch E-E 1985 *Phys. Rev.* B **31** 3795
[6] Straub D, Ley L and Himpsel F J 1985 *Phys. Rev. Lett.* **54** 142
[7] Himpsel F J, Heimann P and Eastman D E 1981 *Phys. Rev.* B **24** 2003
[8] Ortega J E and Himpsel F J 1993 *Phys. Rev.* B **47** 2130
[9] Mašović D R, Vukajlović F R and Zeković S 1983 *J. Phys. C: Solid State Phys.* **16** 6731
[10] Chan C T, Vanderbilt D and Louie S G 1986 *Phys. Rev.* B **33** 2455
[11] Rohlfing M, Krüger P and Pollmann J 1993 *Phys. Rev.* B **48** 17 791
[12] Kheifets A S and Cai Y Q 1995 *J. Phys.: Condens. Matter* **7** 1821
[13] Williamson A J, Hood R Q, Needs R J and Rajagopal G 1998 *Phys. Rev.* B **57** 12 140
[14] Coplan M A, Moore J H and Doering J P 1994 *Rev. Mod. Phys.* **66** 985
McCarthy I E and Weigold E 1991 *Rep. Prog. Phys.* **54** 789
[15] McCarthy I E and Weigold E 1988 *Rep. Prog. Phys.* **51** 299
Dennison J R and Ritter A L 1996 *J. Electron. Spectrosc. Relat. Phenom.* **77** 99
[16] For example: Vos M and McCarthy I E 1995 *J. Electron. Spectrosc. Relat. Phenom.* **74** 15
Fang Z, Guo X, Canney S A, Utteridge S, Ford M J, McCarthy I E, Kheifets A S, Vos M and Weigold E 1998 *Phys. Rev.* B **57** 4349
[17] Vos M, Storer P, Canney S A, Kheifets A S, McCarthy I E and Weigold E 1994 *Phys. Rev.* B **50** 5635
[18] Fang Z, Matthews R S, Utteridge S, Vos M, Canney S A, Gao X, McCarthy I E and Weigold E 1998 *Phys. Rev.* B **57** 12 882
[19] Vos M, Storer P, Cai Y Q, Kheifets A S, McCarthy I E and Weigold E 1995 *J. Phys.: Condens. Matter* **7** 279
[20] Storer P, Caprari R S, Clark S A C, Vos M and Weigold E 1994 *Rev. Sci. Instrum.* **65** 2214
Canney S A, Brunger M J, McCarthy I E, Storer P J, Utteridge S, Vos M and Weigold E 1997 *J. Electron. Spectrosc. Relat. Phenom.* **83** 65
[21] Utteridge S J, Sashin V A, Canney S A, Ford M J, Fang Z, Oliver D R, Vos M and Weigold E 1999 *Appl. Surf. Sci.* to be published
[22] Skriver H L 1984 *The LMTO Method* (Berlin: Springer)
[23] Glötzel D, Segall R and Anderson O K 1980 *Solid State Commun.* **36** 403
[24] Cohen M L and Chelikowsky J R 1988 *Electronic Structure and Optical Properties of Semiconductors* (Berlin: Springer)
[25] Canney S A, Sashin V A, Ford M J and Kheifets A S 1999 *J. Phys.: Condens. Matter* **11** 7507
[26] Canney S A, Vos M, Kheifets A S, Clisby N, McCarthy I E and Weigold E 1997 *J. Phys.: Condens. Matter* **9** 1931
[27] Chelikowsky J R and Cohen L 1976 *Phys. Rev.* B **14** 4450
[28] Hellwege K-H and Madelung O 1982 *Numerical Data and Functional Relationships in Science and Techology* vols 17a and 22a (Berlin: Springer)
[29] Spicer W E and Eden R C 1968 *Proc. 9th Int. Conf. on the Physics of Semiconductors (Moscow, 1968)* vol 1, ed S M Ryvkin (Leningrad: Nauka) p 65